Article

Nuclear Magnetic Shielding and Quadrupole Coupling Tensors in Liquid Water: A Combined Molecular Dynamics Simulation and Quantum Chemical Study

Teemu S. Pennanen, Juha Vaara, Perttu Lantto, Atte J. Sillanp, Kari Laasonen, and Jukka Jokisaari

J. Am. Chem. Soc., **2004**, 126 (35), 11093-11102• DOI: 10.1021/ja048049i • Publication Date (Web): 12 August 2004

J|A|C|S
ARTICLES
Published on Web 08/12/2004

Nuclear Magnetic Shielding and Quadrupole Coupling Tensors in Liquid Water: A Combined Molecular Dynamics Simulation and Quantum Chemical Study

Teemu S. Pennanen,*,†,‡ Juha Vaara,*,‡ Perttu Lantto,† Atte J. Sillanpää,§ Kari Laasonen,§ and Jukka Jokisaari†

Contribution from NMR Research Group, Department of Physical Sciences, P.O. Box 3000, FIN-90014, University of Oulu, Finland; Laboratory of Physical Chemistry, Department of Chemistry, P.O. Box 55 (A.I.Virtasen aukio1), FIN-00014, University of Helsinki, Finland; Laboratory of Physical Chemistry, Department of Chemistry, P.O. Box 3000, FIN-90014, University of Oulu, Finland

Received April 5, 2004; E-mail: tepennan@paju.oulu.fi; jvaara@chem.helsinki.fi

Abstract: Nuclear magnetic resonance (NMR) shielding tensors for the oxygen and hydrogen nuclei, as well as nuclear quadrupole coupling tensors for the oxygen and deuterium nuclei of water in the liquid and gaseous state, are calculated using Hartree−Fock and density functional theory methods, for snapshots sampled from Car−Parrinello molecular dynamics trajectories. Clusters representing local liquid structures and instantaneous configurations of a single molecule representing low-density gas are fed into a quantum chemical program for the calculation of the NMR tensors. The average isotropic and anisotropic tensorial properties of 400 samples in both states, averaged using a common Eckart coordinate frame, are calculated from the data. We report results for the gas-to-liquid chemical shifts of ^{17}O and ^{1}H nuclei, as well as the corresponding change in the nuclear quadrupole couplings of ^{17}O and ^{2}H. Full thermally averaged shielding and quadrupole coupling tensors are reported for the gaseous and liquid-state water, for the first time in the case of liquid. Electron correlation effects, the difference of classical vs quantum mechanical rovibrational averaging, and different methods of averaging anisotropic properties are discussed.

1. Introduction

Realistic comparison of experimentally and theoretically calculated nuclear magnetic resonance (NMR) parameters requires the modeling of thermal and solvent effects.[1] Conventionally, quantum chemical (QC) calculations are carried out for single molecules in vacuo and at the equilibrium geometry, hence not taking rovibrational or environmental effects into account. A straightforward means of including solvation and motional effects is to use, for example, molecular dynamics (MD) simulations to produce instantaneous configurations for the system of interest. Based on these configurations, electronic properties such as the NMR parameters can be calculated "on the fly" using the same periodic framework of electronic structure calculation as used for generating the dynamical trajectory. This is in principle the method followed in the Car−Parrinello molecular dynamics (CPMD)/density functional theory (DFT) method of Sebastiani and Parrinello.[2] A related approach has been forwarded by Mauri, Pfrommer, and Louie.[3] Alternatively, configurations generated by using suitable empirical or nonempirical potentials in a separate simulation program may be fed into a conventional QC step for the property calculation. This approach has been pioneered by Huber and co-workers.[4−9] In either case, the combined time and ensemble average of the instantaneous NMR properties can be compared with the experimental observables.

The difference between nuclear magnetic shielding constants in liquid and gaseous states, the gas-to-liquid shift, is a sensitive measure of the intermolecular interactions and is experimentally well-known for protons[10,11] and oxygen[12,13] in water, which thus constitutes an excellent test for computational methods.[2,7,8,14−16] Furthermore, the ^{17}O signal in liquid water is generally used as an NMR chemical shift reference for this nucleus.

† Department of Physical Sciences, University of Oulu.
‡ Department of Chemistry, University of Helsinki.
§ Department of Chemistry, University of Oulu.

(1) Helgaker, T.; Jaszuński, M.; Ruud, K. *Chem. Rev.* **1999**, *99*, 293.
(2) Sebastiani, D.; Parrinello, M. *J. Phys. Chem. A* **2001**, *105*, 1951.
(3) Mauri, F.; Pfrommer, B. G.; Louie, S. G. *Phys. Rev. Lett.* **1996**, *77*, 5300.
(4) Eggenberger, R.; Gerber, S.; Huber, H.; Searles, D.; Welker, M. *J. Chem. Phys.* **1992**, *97*, 5898.
(5) Eggenberger, R.; Gerber, S.; Huber, H.; Searles, D.; Welker, M. *Mol. Phys.* **1993**, *80*, 1177.
(6) Eggenberger, R.; Gerber, S.; Huber, H.; Searles, D.; Welker, M. *J. Comput. Chem.* **1993**, *14*, 1553.
(7) Malkin, V. G.; Malkina, O. L.; Steinebrunner, G.; Huber, H. *Chem.—Eur. J.* **1996**, *2*, 452.
(8) Searles, D. B.; Huber, H. In *Encyclopedia of Nuclear Magnetic Resonance, Volume 9: Advances in NMR*; Grant, D. M., Harris, R. K., Eds.; John Wiley & Sons: Ltd: Chichester, 2002.
(9) Hardy, E. H.; Müller, M. G.; Vogt, P. S.; Bratschi, C.; Kirchner, B.; Huber, H.; Searles, D. J. *J. Chem. Phys.* **2003**, *119*, 6184.
(10) Hindman, J. C. *J. Chem. Phys.* **1966**, *44*, 4582.
(11) Raynes, W. T. In *Nuclear Magnetic Resonance, A Specialist Periodical Report*; Royal Society of Chemistry: London, 1978; Vol. 7, p 1.
(12) Florin, A.; Alei, M., Jr. *J. Chem. Phys.* **1967**, *47*, 4268.
(13) Raynes, W. T. *Mol. Phys.* **1983**, *49*, 443.
(14) Chesnut, D. B.; Rusiloski, B. E. *THEOCHEM* **1994**, *314*, 19.
(15) Pfrommer, B. G.; Mauri, F.; Louie, S. G. *J. Am. Chem. Soc.* **2000**, *122*, 123.
(16) Cossi, M.; Crescenzi, O. *J. Chem. Phys.* **2003**, *118*, 8863.

10.1021/ja048049i CCC: $27.50

Computational averaging of anisotropic molecular properties is rarely done, although it provides experimentally unattainable information such as individual components of the shielding and quadrupole coupling tensors. The averaging requires the tensors to be represented in the Eckart frame,[17] an appropriate coordinate system which remains fixed at the molecule, when component-wise accumulation of individual tensor components is carried out.[18−20]

Experimental proton shielding anisotropy in liquid water has recently been measured by Modig and Halle[21] using relaxation data. For protons in ice, there exist a few measurements.[22−25] There are no experimental reports of the shielding anisotropy of water in the gaseous state. Instead, one can use computational ab initio results for a single molecule[20] to represent the gaseous state value in estimating the effect of solvation on the shielding anisotropy. Such estimations are better made by using similar methodologies for the different states of the medium, though.

In this paper, we investigate the problem of a single water molecule solvated in liquid-state water and in the gas phase. We follow the second computational approach outlined above and generate configurations of liquid water and one "gas-phase" water molecule in nonempirical CPMD simulations. The generated liquid-state trajectory is sampled by cutting roughly spherical clusters including the central molecule and its neighborhood out of the simulation snapshots, to be subsequently used as an input for QC calculations of NMR properties. The properties to be calculated are the nuclear magnetic shielding tensors of the oxygen nucleus and the protons and the nuclear quadrupole coupling tensors of oxygen and deuterium nuclei. We use the Eckart frame to facilitate reliable extraction of the tensors from the instantaneous configurations. Experimentally measurable parameters are calculated from the average tensors. The shielding calculations use the gauge-including atomic orbital (GIAO) ansatz[26,27] with the Hartree−Fock (HF) and DFT methods.

2. Theory

Nuclear magnetic shielding is a measure of the modification of the external magnetic field at the site of the nucleus, caused by the electron distribution.[28−30] Hence, the shielding carries information about the electronic and molecular structure. The most commonly determined spectral parameter in NMR experiments carried out in isotropic liquids is the nuclear magnetic shielding constant, one-third of the trace of the time-averaged shielding tensor. In terms of the spin-Hamiltonian approach, the shielding tensor is defined as the energy derivative with respect to the nuclear magnetic moment, $\boldsymbol{\mu}$, of this nucleus and the magnetic field, $\mathbf{B}$, at the site of the nucleus, evaluated at $\boldsymbol{\mu} = \mathbf{0}$ and $\mathbf{B} = \mathbf{0}$.[1]

Nuclear quadrupole coupling describes the interaction between the nuclear electric quadrupole moment and the electric field gradient (EFG) at the site of the nucleus.[28,29,31] The quadrupole coupling thus also provides information about the molecular environment of the nucleus. The determination of the nuclear quadrupole coupling constant (NQCC), time-average of the largest principal component of the nuclear quadrupole coupling tensor, is usually based on NMR relaxation time measurements in liquids.

Nuclear magnetic shielding and EFG tensors are modified when going from the gaseous to liquid state. This is due to both solvation and the difference in the rovibrational effects in the two states. The observable A, which can be the shielding or quadrupole coupling constant or any combination of the tensor components, in the gaseous and liquid states can be written as

$$A(\mathrm{g}) = A(\mathrm{e}) + A(\mathrm{g})_{\mathrm{rovib}} + A(\mathrm{g})_{\mathrm{envir}} \quad (1)$$

$$A(\mathrm{l}) = A(\mathrm{e}) + A(\mathrm{l})_{\mathrm{rovib}} + A(\mathrm{l})_{\mathrm{envir}} \quad (2)$$

where $A(\mathrm{e})$ is the value of A in a single noninteracting molecule at the equilibrium geometry, $A(\mathrm{g})_{\mathrm{rovib}}$ and $A(\mathrm{l})_{\mathrm{rovib}}$ arise due to the rovibrational effects in the gaseous and liquid states, respectively, and $A(\mathrm{g})_{\mathrm{envir}}$ and $A(\mathrm{l})_{\mathrm{envir}}$ are the contributions due to the environment of the molecule in gaseous and liquid states, respectively. We assume that the environmental effects in the gas phase are negligible, i.e., $A(\mathrm{g})_{\mathrm{envir}} \approx 0$. Hence, the gas-to-liquid shift can be written as

$$A_{\mathrm{gas-to-liquid}} = A(\mathrm{l}) - A(\mathrm{g}) = A(\mathrm{l})_{\mathrm{envir}} + [A(\mathrm{l})_{\mathrm{rovib}} - A(\mathrm{g})_{\mathrm{rovib}}] \quad (3)$$

Classical approximations for the rovibrational contributions in both states, as well as the environmental contribution for the liquid state, are obtained by averaging over configurations generated by MD simulations. The true quantum mechanical rovibrational effects, most importantly those due to the zero-point vibrational motion, are not included in this method. However, it is assumed that the errors thus made for the gaseous and liquid states cancel in the difference $[A(\mathrm{l})_{\mathrm{rovib}} - A(\mathrm{g})_{\mathrm{rovib}}]$.

Nuclear magnetic shielding and quadrupole coupling are tensorial properties. The tensorial character is not displayed, however, in static NMR experiments when the reorientational motion of the molecules is isotropic. Only the differences between shielding constants, the chemical shifts, are then available. Anisotropic shielding and quadrupole coupling constants can be observed in the static spectral parameters in solid-state and liquid-crystal experiments, as well as in the relaxation rates.

When averaging anisotropic molecular properties, such as individual components of the shielding or quadrupole coupling tensors, over molecular rotations and vibrations, a consistent Eckart coordinate frame for representing the tensors must be selected.[17] While an arbitrary frame can initially be chosen, the Eckart conditions are required for the coordinate frame used for representing each subsequent instantaneous conformation

(17) Eckart, C. *Phys. Rev.* **1935**, *47*, 552.
(18) Louck, J. D.; Galbraith, H. W. *Rev. Mod. Phys.* **1976**, *48*, 69.
(19) Fowler, P. W.; Raynes, W. T. *Mol. Phys.* **1981**, *43*, 65.
(20) Vaara, J.; Lounila, J.; Ruud, K.; Helgaker, T. *J. Chem. Phys.* **1998**, *109*, 8388.
(21) Modig, K.; Halle, B. *J. Am. Chem. Soc.* **2002**, *124*, 12031.
(22) Pines, A.; Ruben, D. J.; Vega, S.; Mehring, M. *Phys. Rev. Lett.* **1976**, *36*, 110.
(23) Ryan, L. M.; Wilson, R. C.; Gernstein, B. C. *Chem. Phys. Lett.* **1977**, *52*, 341.
(24) Burum, D. P.; Rhim, W. K. *J. Chem. Phys.* **1979**, *70*, 3553.
(25) Rhim, W. K.; Burum, D. P.; Elleman, D. D. *J. Chem. Phys.* **1979**, *71*, 3139.
(26) Wolinski, K.; Hinton, J. F.; Pulay, P. *J. Am. Chem. Soc.* **1990**, *112*, 8251.
(27) Helgaker, T.; Jørgensen, P. *J. Chem. Phys.* **1991**, *95*, 2595.
(28) Abragam, A. *The Principles of Nuclear Magnetism*; Oxford University Press: Oxford, 1961.
(29) Slichter, C. P. *Principles of Magnetic Resonance*, 2nd ed; Springer: Berlin, 1990.
(30) Ramsey, N. F. *Phys. Rev.* **1950**, *78*, 699.
(31) Pound, R. V. *Phys. Rev.* **1950**, *79*, 685.

of the molecule. The Eckart frame remains fixed at the molecule during its rotations and vibrations in such a way that the coupling between the rotational and vibrational degrees of freedom is minimized.[18] The conditions define molecule-fixed axes in terms of the instantaneous position vectors of the nuclei in the molecule, $\{\mathbf{r}_K\}$, and can be derived by requiring that the angular momentum of the nuclei relative to the molecule-fixed axes vanishes when the nuclei are at their equilibrium positions (when $\mathbf{r}_K = \mathbf{r}_K^e$). These conditions are

$$\sum_K m_K \mathbf{r}_K^e \times \mathbf{r}_K = \mathbf{0} \tag{4}$$

where m_K is the mass of nucleus K. The Eckart coordinate system is a Cartesian coordinate system which has its origin at the instantaneous center of mass and whose axes are aligned so that eq 4 holds. The essential point here is that the Eckart frame is uniquely defined by the three sets of parameters $\mathbf{r}_K^e$, $\mathbf{r}_K$, and m_K.

3. Computational Methods

3.1. Simulation Trajectory. The water trajectories were generated using the Car−Parrinello molecular dynamics method[32] with the FINGER[33] code. In the method, the nuclear dynamics is treated classically but the forces acting on the nuclei are calculated quantum mechanically from the electronic structure, using DFT. Two simulation trajectories were used, one for the liquid state and another for the gaseous state of water. The simulations were carried out for the isotopomer $^1H_2{}^{16}O$. The change from the NMR-active nucleus ^{17}O to ^{16}O causes changes in the dynamical behavior of the molecules. However, as we have studied, using classical dynamics, magnetic properties dependent on the water structure in this contribution, the change of the isotopomer does not have an effect on the calculated results. In both trajectories, the intramolecular geometries of all the water molecules were allowed to evolve freely. The liquid simulation contained 32 water molecules in a cubic simulation box with the lengths of all sides equal to 18.62 au, producing the density 1.000 g cm^{-3}. Between Car−Parrinello simulations of liquid water using 64 vs 32 molecules, the structural properties of the liquid were found to change relatively little.[34] In particular, the electric dipole moment of an individual molecule, which is a global molecular property, only changed by about 2% between the two simulations. Hence, we believe that the model with 32 molecules is adequate for the presently considered, very local molecular properties. The gas-phase simulation contained one molecule in a cubic box with sides 12.2 au. Both simulations used the BLYP[35,36] exchange correlation functional, Vanderbilt pseudopotentials for both oxygen and hydrogen,[37] and a plane wave cutoff energy of 24 Ry. The time step in integrating the equations of motion was 0.12 fs, and the fictitious mass parameter for the electrons was $\mu = 600$ au. The simulations were performed in the microcanonical *NVE* (constant particle number, volume, and energy) ensemble without constraints, the temperature fluctuating around 300 K. The initial configuration for our liquid simulation was taken from the final configuration of a former, lengthy CPMD simulation for D_2O [with its initial configuration, in turn, being a final configuration of a Becke-only 4 ps water simulation].[38] The gas-phase simulation was started from a configuration close to the equilibrium geometry. In both simulations, the temperature of the nuclear framework was gradually heated to 300 K within 0.05 ps from the start by scaling the atomic velocities. The lengths of the thermalization and production phases were about 1.2 ps and 3 ps for the liquid and about 4 ps and 5 ps for the gas. The radial distribution functions obtained from these simulations, as with BLYP/CPMD simulations in general,[39] agree well with the experimental results.[40]

3.2. Quantum Chemical Calculations. Nearly spherical clusters of molecules were cut out from the simulated liquid-state trajectory and used as an input for the QC calculations. Each cluster contained a central molecule and a suitable neighborhood of molecules around it. A distance criterion was used to determine the neighbors of the central molecule. The molecules that were included had at least one of their atoms inside a sphere (of a chosen radius) centered at the oxygen nucleus of the central molecule.

Many snapshots are needed for statistical convergence of the results. Hence, for clusters large enough, large basis sets cannot be used. To reduce the number of basis functions, the locally dense basis set concept[41,42] was used with different basis sets employed for the central molecule, the nearest neighbors, and the rest of the molecules. The single gas-state molecule was treated at the aug-cc-pVDZ[43] level, which was found suitable for intermolecular effects on nuclear shielding in the water dimer by Pecul et al.[44] This was also the basis set for the central molecule in the liquid calculations. Smaller sets were used for the surrounding molecules as discussed below in section 4.1.

To take care of the long-range electrostatic effects, a reaction field model[45] was used in the liquid-state QC calculations. The clusters were placed in a spherical cavity cut into a dielectric continuum. The radius of the cavity equaled the distance between the center of mass of the cluster and its most distant atom plus the van der Waals radius of this atom. The dielectric constant $\epsilon_r = 78.5$, appropriate for water, was chosen for the continuum.

QC calculations (400) for both liquid clusters and gas samples were performed with the DALTON electronic structure program,[46] using the HF and DFT methods, the latter in order to roughly estimate the effect of electron correlation. Both use the GIAO ansatz. The hybrid B3LYP functional[47] was chosen for the DFT calculations. The HF implementation is that of Ruud et al.,[48] and the DFT one is by Helgaker et al.[49]

3.3. Sampling and Estimation of Statistical Errors. We aimed at balanced treatment of all error sources affecting the final results. It is useless to treat one aspect of the modeling with high precision if the other steps dominate the error. The size of the statistical sample was chosen such that a similar order of magnitude was obtained for the statistical (vide infra) and systematic errors, the latter originating in the basis set deficiencies, incomplete electron correlation treatment, finite cluster size, the use of a classical trajectory, and so on.

(32) Car, R.; Parrinello, M. *Phys. Rev. Lett.* **1985**, *55*, 2471.
(33) The FINGER-program has mainly been developed in the Helsinki University of Technology, Espoo, Finland. It is based largely on techniques presented in the paper by Laasonen, K.; Pasquarello, A.; Car, R.; Lee, C.; Vanderbilt, D. *Phys. Rev. B* **1993**, *47*, 10142.
(34) Silvestrelli, P. L.; Parrinello, M. *J. Chem. Phys.* **1999**, *111*, 3572.
(35) Becke, A. D. *Phys. Rev. A* **1988**, *38*, 3098.
(36) Lee, C.; Yang, W.; Parr, R. *Phys. Rev. B* **1988**, *37*, 785.
(37) Vanderbilt, D. *Phys. Rev. B.* **1990**, *41*, 5048. Laasonen, K.; Car, R.; Lee, C.; Vanderbilt, D. *Phys. Rev. B* **1991**, *43*, 6796.
(38) Laasonen, K.; Sprik, M.; Parrinello, M. *J. Chem. Phys.* **1993**, *99*, 9080.
(39) Silvestrelli, P. L.; Parrinello, M. *Phys. Rev. Lett.* **1999**, *82*, 3308.
(40) Soper, A. K.; Bruni, F.; Ricci, M. A. *J. Chem. Phys.* **1997**, *106*, 247. Narten, A. H.; Levy, H. A. *J. Chem. Phys.* **1971**, *55*, 2263.
(41) Chesnut, D. B.; Moore, K. D. *J. Comput. Chem.* **1989**, *10*, 648.
(42) Chesnut, D. B.; Rusiloski, B. E.; Moore, K. D.; Egolf, D. A. *J. Comput. Chem.* **1993**, *14*, 1364.
(43) Dunning, T., Jr. *J. Chem. Phys.* **1989**, *90*, 1007.
(44) Pecul, M.; Lewandowski, J.; Sadlej, J. *Chem. Phys. Lett.* **2001**, *333*, 139.
(45) Mikkelsen, K.; Jørgensen, P.; Ruud, K.; Helgaker, T. *J. Chem. Phys.* **1997**, *106*, 1170.
(46) Helgaker, T.; Jensen, H. J. Aa.; Jørgensen, P.; Olsen, J.; Ruud, K.; Ågren, H.; Bak, K. L.; Bakken, V.; Christiansen, O.; Coriani, S.; Dahle, P.; Dalskov, E. K.; Enevoldsen, T.; Fernandez, B.; Hættig, C.; Hald, K.; Halkier, A.; Heiberg, H.; Hettema, H.; Jonsson, D.; Kirpekar, S.; Kobayashi, R.; Koch, H.; Mikkelsen, K. V.; Norman, P.; Packer, M. J.; Ruden, T. A.; Saue, T.; Sauer, S. P. A.; Schimmelpfennig, B.; Sylvester-Hvid, K. O.; Taylor, P. R.; Vahtras, O. *Dalton release 1.2 2001, an electronic structure program*. See http://www.kjemi.uio.no/software/dalton/dalton.html. The DFT calculations were carried out with a prerelease version 2.0 kindly placed at our disposal by T. Helgaker and P. Sałek.
(47) Becke, A. D. *J. Chem. Phys.* **1993**, *98*, 5648. Stephens, P. J.; Devlin, F. J.; Chabalowski, C. F.; Frisch, M. J. *J. Phys. Chem.* **1994**, *98*, 11623.
(48) Ruud, K.; Helgaker, T.; Kobayashi, R.; Jørgensen, P.; Bak, K.; Jensen, H. J. Aa. *J. Chem. Phys.* **1994**, *100*, 8178.
(49) Helgaker, T.; Wilson, P.; Amos, R.; Handy, N. *J. Chem. Phys.* **2000**, *113*, 2983.

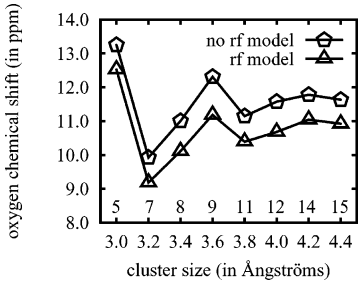

Figure 1. Variation of the Hartree−Fock level chemical shift of the central oxygen nucleus in an example water cluster, with respect to increasing cluster size, and with and without the reaction field model, using the aug-cc-pVDZ basis set. The number of water molecules is indicated below the symbols. The chemical shift reference in this figure is the same central molecule, without the reaction field model and surrounding molecules. In production calculations, the reaction field and the cluster radius 4.2 Å were used.

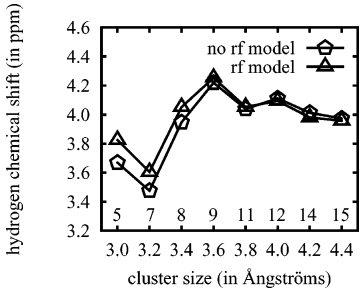

Figure 2. Same conditions as those in Figure 1 but for the proton chemical shift of one of the protons of the central water molecule.

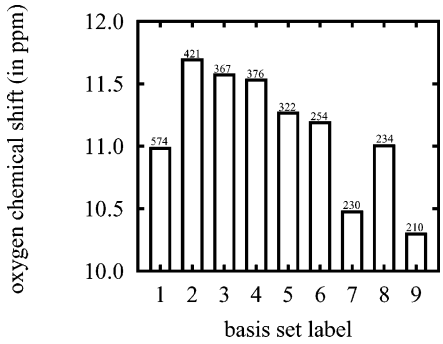

Figure 3. Variation of the chemical shift of the central oxygen nucleus in an example water cluster with respect to different basis sets. Numbering in the horizontal axis corresponds to the following: (1) all molecules with aug-cc-pVDZ; (2) central molecule (CM) and 4 nearest neighbors (4NN) aug-cc-pVDZ, the rest of the molecules (RM) cc-pVDZ; (3) CM + 4NN aug-cc-pVDZ, RM cc-pVDZ without the *p*-functions of hydrogen (-H*p*); (4) CM + 4NN aug-cc-pVDZ, RM cc-pVDZ without the *d*-functions of oxygen (-O*d*); (5) CM + 4NN aug-cc-pVDZ, RM cc-pVDZ-H*p*-O*d*; (6) CM aug-cc-pVDZ, 4NN cc-pVDZ, RM cc-pVDZ-H*p*-O*d*; (7) CM aug-cc-pVDZ, 4NN cc-pVDZ-H*p*, RM cc-pVDZ-H*p*-O*d*; (8) CM aug-cc-pVDZ, 4NN cc-pVDZ-O*d*, RM cc-pVDZ-H*p*-O*d*; (9) CM aug-cc-pVDZ, NN+RM cc-pVDZ-H*p*-O*d*. The number of basis functions (for 14 molecules) is indicated for each calculation. In production calculations, the basis set (8) was used.

Sample snaphots from the simulations were suitably chosen from the equilibrated parts of the trajectories, where the instantaneous temperature fluctuates with the average at 300 K. The liquid samples included many different snapshots, several clusters corresponding to different choice of the central molecule and its neighborhood being selected from each snapshot. Averaging over all these clusters led to the time and ensemble average.

To ensure that the samples used for averaging are not statistically correlated, different central molecules were taken for the calculated clusters. The sampling for the gas molecule was performed with the interval of 100 steps (12 fs), and with the liquid, different sampling intervals were employed. No interval less than 50 steps (6.0 fs) appeared, however. These sampling intervals may be compared to the choice of 2.5 fs in a recent state-of-the-art simulation study of liquid water.[9]

The results are represented as property averages with error limits. The error limit σ, the standard deviation of the mean value, is calculated as the square root of the variance of the mean value,

$$\sigma = \sqrt{\frac{1}{N^2}\sum_{i=1}^{N}(A_i - \langle A\rangle)^2} \qquad (5)$$

where $\langle A\rangle$ is the mean value of A and N is the number of samples. The calculation of the mean values and their error limits for scalar quantities is straightforward. For anisotropic properties, the search of the Eckart coordinate frame was performed separately for the central molecule of each snapshot cluster. When all the property tensors were transformed to the Eckart frame,[20] the averaging and calculation of error limits were performed in the same manner as that for the scalars. All the calculations and transformations were automated.

4. Results and Discussion

4.1. Test Calculations. Figure 1 displays the ^{17}O chemical shift for the central molecule of an example cluster, performed at the HF level with the aug-cc-pVDZ basis, when the radius of the cluster is increased from 3.0 Å to 4.4 Å. Increasing the radius of the cluster beyond 4.2 Å has only a small effect on the environmental contribution to the chemical shift of the central oxygen. In this test calculation, this radius corresponds to a cluster of 14 molecules (central molecule + 13 neighbors). In the production calculations, this choice yielded clusters with sizes ranging from 10 to 19 molecules, depending on the case. The clusters contained about 15 molecules on average, thus much of the second solvation shell of water is explicitly considered. In the calibration snapshot, the smallest cluster with the radius of 3.0 Å is a pentamer yielding a shift of about 1.5 ppm removed from the converged value at 4.2 Å. However, quite large oscillations in the chemical shift occur before convergence. For comparison, the shifts obtained with the reaction field surrounding each cluster are shown. This contribution affects the shift by about 0.7 ppm for the 4.2 Å cluster, showing that long-range electrostatic effects are important when accurate ^{17}O chemical shifts are pursued. The cluster radius of 4.2 Å was also used in the recent simulation of ^{2}H quadrupole coupling in liquid water in ref 9.

The respective behavior of one of the hydrogens of the central molecule in the same test case is shown in Figure 2. The shift for the pentamer is less than 0.4 ppm off from the nearly converged value at a 4.2 Å cutoff, the intermediate region showing again large oscillations. The shift caused by the reaction field is only about 0.03 ppm, i.e. relatively smaller than for oxygen. The reaction field contribution for hydrogen is large for the pentamer but decreases with increasing size of the cluster. In contrast, for ^{17}O, this effect is practically identical for the pentamer and the 4.2 Å cluster.

To select the basis set for the production calculations, test calculations were performed for the example cluster at the HF level. Figures 3 and 4 display the ^{17}O and ^{1}H chemical shifts, respectively, for the central molecule of the 4.2 Å cluster, when different basis sets are used along with the reaction field model. The changes from the aug-cc-pVDZ used for all molecules (basis

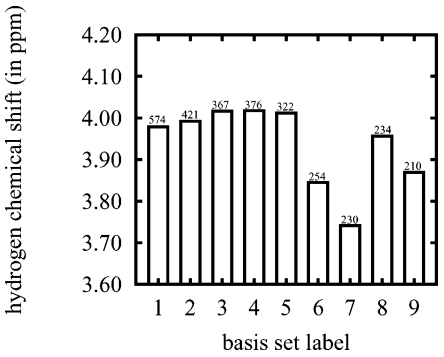

Figure 4. Same conditions as those in Figure 3 but for the hydrogen nucleus.

1) to different locally dense bases were performed one change at a time. For example, the switch from basis 1 to basis 2 involves changing the basis used for the outer neighbors from aug-cc-pVDZ to cc-pVDZ, and the switch from basis2 to basis 3 means the removal of the *p*-type hydrogen functions from the cc-pVDZ basis of the outer neighbors and so on.

For oxygen (Figure 3), changing the basis set of the outer neighbors leads to significant chemical shift changes. Removing the *p*-type hydrogen functions from the nearest neighbors (basis 7) deteriorates the chemical shift of the central molecule too much. Instead, removing the *d*-type oxygen functions of the nearest neighbors (basis 8) leads economically [234 functions for $(H_2O)_{14}$] to acceptable accuracy. For this specific cluster, a very close match is obtained with the results of using aug-cc-pVDZ throughout.

For hydrogen (Figure 4), the change of the basis of the outer neighbors has little significance, but the changes in the nearest neighbors' basis influences the chemical shift quite substantially. As for ^{17}O, a reasonable compromise between accuracy and cost is obtained with basis 8, where the *d*-type oxygen functions are removed from the cc-pVDZ basis of the nearest neighbors.

In summary, basis set 8 is chosen for the production calculations. In it, the central molecule is treated at the aug-cc-pVDZ level, the nearest neighbors (chosen by a similar distance criterion of 2.5 Å as before) with cc-pVDZ with the *d*-type oxygen functions removed, and the rest of the molecules with cc-pVDZ with both the *d*-type oxygen functions and the *p*-type hydrogen functions removed.

For the use of the reaction field model, we optimized the order of the multipole expansion. Test calculations show that any value from 1 to 10 can be used with only very little effect on the results and with little effect on the computational time. The value 6 was chosen.

4.2. Shielding Constants and Gas-to-Liquid Shift in Water. Our results for the nuclear magnetic shielding constants of oxygen and hydrogen nuclei in liquid and gaseous water at 300 K, as well as the difference, the gas-to-liquid shift, are shown in Tables 1 and 2. Other computational and experimental results are also shown. Our quoted error limits are purely statistical and do not include other sources of error due to, for example, the incompleteness of the basis set and electron correlation treatment, the finite size of the clusters, or the errors in the geometries due to the classical simulation. The error in the gas-to-liquid shift is the sum of the statistical errors of the shielding constants in the liquid and gaseous states.

Our HF and B3LYP results for the ^{17}O gas-to-liquid shift are -24.3 ± 1.4 ppm and -41.2 ± 1.5 ppm, respectively. The

Table 1. Calculated and Experimental ^{17}O Nuclear Shielding Constant and Gas-to-Liquid Shift in Water[a]

method	σ(g)	σ(l)	$\delta = \sigma(l) - \sigma(g)$
HF[b]	311.0 ± 0.9	286.7 ± 0.6	-24.3 ± 1.4
B3LYP[b]	309.7 ± 0.9	268.5 ± 0.6	-41.2 ± 1.5
expt	323.6 ± 0.6[c]	287.5 ± 0.6	-36.1[d]
HF[e]			-20.3 ± 9.6
HF[f]	336.6	320.2	-16.4
LDA[g]			-36.6 ± 0.5
PW91[h]			-37.6 ± 2.1
PBE0[i]			-34.8
BLYP[j]			-30
RASSCF[k]	324.0 ± 1.5		

[a] In ppm. [b] Present work, with 400 samples taken from a CPMD trajectory. The error limits correspond to one standard deviation of the mean value. The values of the ^{17}O shielding constant at the equilibrium geometry ($r_{OH} = 0.998$ Å; $\angle_{HOH} = 103.9°$, pertinent to the BLYP/CPMD method used for generating the dynamical trajectories) are 314.8 ppm with HF and 313.6 ppm with B3LYP. [c] Reference 50 based on the experimental determination of the spin-rotation constant of ^{17}O in carbon monoxide $^{12}C^{17}O$,[51] combined with a computational determination of the diamagnetic shielding constant from ref 52 and the experimental chemical shift between CO and H_2O. The error limit is the experimental error in the measurement of the spin-rotation constant. [d] Reference 13. [e] Reference 14 using 30 decamers from MD simulation. [f] Reference 53. Static cluster model where the central molecule was explicitly solvated by four surrounding molecules and a dielectric continuum. [g] Reference 15. Including 9 snapshots containing the whole MD simulation cell of 32 molecules. The reference is a single molecule at the equilibrium geometry. [h] Reference 7. Extrapolated cluster calculations (40 clusters) sampled from an MD trajectory generated using an empirical potential energy function. [i] Reference 16. Using a mixed explicit/continuum solvation model. Clusters of 11 molecules were taken from an MD simulation with the molecules kept at the fixed, optimized geometry. Neither the exact number of the clusters nor the error limits were quoted. [j] Reference 2. No error limits were given in the article. [k] Reference 20. Contains a quantum mechanically calculated rovibrational correction of -12.04 ppm (for the $^1H_2{}^{17}O$ isotopomer).

Table 2. Calculated and Experimental ^1H Nuclear Shielding Constant and Gas-to-Liquid Shift in Water[a]

method	σ(g)	σ(l)	$\delta = \sigma(l) - \sigma(g)$
HF[b]	29.52 ± 0.06	24.38 ± 0.09	-5.14 ± 0.14
B3LYP[b]	30.07 ± 0.05	24.80 ± 0.08	-5.27 ± 0.13
expt[c]	30.052 ± 0.015	25.79	-4.26
HF[d]			-2.28 ± 1.61
HF[e]	30.91	26.94	-3.97
LDA[f]			-5.83 ± 0.10
PW91[g]			-3.22 ± 0.20
BLYP[h]			-4.1
RASSCF[i]	30.2 ± 0.1		

[a] In ppm. [b] Present work. See footnote *b* in Table 1. The values of the ^1H shielding constant at the equilibrium geometry are 29.68 ppm with HF and 30.21 ppm with B3LYP. [c] References 10 and 11. [d] See footnote *e* in Table 1. [e] See footnote *f* in Table 1. [f] See footnote *g* in Table 1. [g] See footnote *h* in Table 1. [h] See footnote *j* in Table 1. [i] See footnote *k* in Table 1. Contains a quantum mechanically calculated rovibrational correction of -0.549 ppm (for the $^1H_2{}^{17}O$ isotopomer).

experimental result, -36.1 ppm, is closer to the B3LYP result. The experimental shift is within the reported statistical error limits of the computational results of Pfrommer et al.[15] and Malkin et al.[7] In the former calculation, the gas-state value was adopted from a molecule at rest at its equilibrium geometry and not from a true rovibrational average. According to our calculations (vide infra), the systematic error thus made in the gas-to-liquid shift amounts to about -4 ppm due to this procedure. For hydrogen, the results of refs 7 and 15 are not very close to the experimental value, one underestimating and the other overestimating the shift. Both our ^1H results (Table 2) overestimate the shift about 1 ppm, being within the error limits of each other. Numerically the best result for ^1H is obtained by Sebastiani and Parrinello[2] using the CPMD method

$$\boldsymbol{\sigma}^{\mathrm{HF}}_{^{17}\mathrm{O}}(e) = \begin{pmatrix} 349.4 & 0.0 & 0.0 \\ 0.0 & 300.1 & 0.0 \\ 0.0 & 0.0 & 294.9 \end{pmatrix}$$

$$\boldsymbol{\sigma}^{\mathrm{HF}}_{^{17}\mathrm{O}}(g) = \begin{pmatrix} 344.7 \pm 0.9 & 0.0 \pm 0.5 & 0.0 \pm 0.0 \\ 0.0 \pm 0.4 & 296.3 \pm 1.0 & 0.0 \pm 0.0 \\ 0.0 \pm 0.0 & 0.0 \pm 0.0 & 292.0 \pm 0.9 \end{pmatrix}$$

$$\boldsymbol{\sigma}^{\mathrm{HF}}_{^{17}\mathrm{O}}(l) = \begin{pmatrix} 309.7 \pm 0.8 & -0.2 \pm 0.5 & 0.0 \pm 0.4 \\ 0.4 \pm 0.5 & 277.7 \pm 0.7 & 0.0 \pm 0.4 \\ 0.1 \pm 0.2 & 0.1 \pm 0.3 & 272.8 \pm 0.6 \end{pmatrix}$$

$$\boldsymbol{\sigma}^{\mathrm{B3LYP}}_{^{17}\mathrm{O}}(e) = \begin{pmatrix} 346.6 & 0.0 & 0.0 \\ 0.0 & 303.7 & 0.0 \\ 0.0 & 0.0 & 290.4 \end{pmatrix}$$

$$\boldsymbol{\sigma}^{\mathrm{B3LYP}}_{^{17}\mathrm{O}}(g) = \begin{pmatrix} 341.7 \pm 1.0 & 0.0 \pm 0.5 & 0.0 \pm 0.0 \\ 0.0 \pm 0.4 & 300.0 \pm 0.9 & 0.0 \pm 0.0 \\ 0.0 \pm 0.0 & 0.0 \pm 0.0 & 287.5 \pm 0.9 \end{pmatrix}$$

$$\boldsymbol{\sigma}^{\mathrm{B3LYP}}_{^{17}\mathrm{O}}(l) = \begin{pmatrix} 290.7 \pm 0.8 & 0.3 \pm 0.5 & 0.0 \pm 0.4 \\ 0.7 \pm 0.5 & 261.7 \pm 0.8 & 0.0 \pm 0.4 \\ 0.1 \pm 0.2 & 0.1 \pm 0.4 & 253.2 \pm 0.7 \end{pmatrix}$$

Figure 5. ^{17}O nuclear magnetic shielding tensors $\boldsymbol{\sigma}$ (in ppm) in water at the equilibrium geometry (e) and thermally averaged in gas (g) and liquid (l) phase at 300 K. The molecule is in the *xy* plane, with the C_2 axis in the *y* direction.

$$\boldsymbol{\sigma}^{\mathrm{HF}}_{^{1}\mathrm{H}}(e) = \begin{pmatrix} 36.84 & 8.29 & 0.00 \\ 6.70 & 29.31 & 0.00 \\ 0.00 & 0.00 & 22.89 \end{pmatrix}$$

$$\boldsymbol{\sigma}^{\mathrm{HF}}_{^{1}\mathrm{H}}(g) = \begin{pmatrix} 36.64 \pm 0.07 & 8.16 \pm 0.04 & 0.00 \pm 0.00 \\ 6.53 \pm 0.05 & 29.13 \pm 0.07 & 0.00 \pm 0.00 \\ 0.00 \pm 0.00 & 0.00 \pm 0.00 & 22.79 \pm 0.04 \end{pmatrix}$$

$$\boldsymbol{\sigma}^{\mathrm{HF}}_{^{1}\mathrm{H}}(l) = \begin{pmatrix} 34.36 \pm 0.13 & 12.72 \pm 0.10 & -0.01 \pm 0.06 \\ 11.90 \pm 0.10 & 24.20 \pm 0.14 & -0.07 \pm 0.05 \\ -0.03 \pm 0.07 & -0.05 \pm 0.05 & 14.58 \pm 0.13 \end{pmatrix}$$

$$\boldsymbol{\sigma}^{\mathrm{B3LYP}}_{^{1}\mathrm{H}}(e) = \begin{pmatrix} 37.12 & 7.86 & 0.00 \\ 5.62 & 29.73 & 0.00 \\ 0.00 & 0.00 & 23.79 \end{pmatrix}$$

$$\boldsymbol{\sigma}^{\mathrm{B3LYP}}_{^{1}\mathrm{H}}(g) = \begin{pmatrix} 36.93 \pm 0.07 & 7.72 \pm 0.04 & 0.00 \pm 0.00 \\ 5.43 \pm 0.05 & 29.57 \pm 0.07 & 0.00 \pm 0.00 \\ 0.00 \pm 0.00 & 0.00 \pm 0.00 & 23.70 \pm 0.03 \end{pmatrix}$$

$$\boldsymbol{\sigma}^{\mathrm{B3LYP}}_{^{1}\mathrm{H}}(l) = \begin{pmatrix} 34.30 \pm 0.12 & 12.02 \pm 0.09 & -0.01 \pm 0.06 \\ 11.02 \pm 0.10 & 24.60 \pm 0.14 & -0.07 \pm 0.05 \\ -0.03 \pm 0.07 & -0.05 \pm 0.05 & 15.49 \pm 0.13 \end{pmatrix}$$

Figure 6. Same conditions as those in Figure 5 but for ^{1}H nuclear magnetic shielding.

that yields a result only a few tenths of a part per million removed from the experimental value. No error limits are quoted for their results, however.

The electron correlation effect on the gas-to-liquid shift can be estimated by comparing the uncorrelated HF and correlated B3LYP results. Correlation adds about 17 ppm to the ^{17}O gas-to-liquid shift but has only a negligible effect on the ^{1}H shift. Inclusion of correlation is hence verified to be necessary[7] in a reliable calculation of the gas-to-liquid shift of ^{17}O. Due to the varying statistical sample sizes and conventions used when reporting the error limits, as well as other methodological differences between the present calculations and earlier reports, it is not possible to select a preferred exchange-correlation functional based on the DFT data at hand. Our calculations at the HF and B3LYP levels should nevertheless provide faithful and systematic representation of the difference of the performance of these two methods.

The classical rovibrational correction for the gaseous state can be obtained by comparing our ^{17}O and ^{1}H gaseous shielding constants to the shielding constants of the molecule at the equilibrium geometry, optimized with the same parameters as those used in the MD simulation. The corrections for the gaseous state amount to −3.8 ppm and −3.9 ppm for the ^{17}O shielding constant at the HF and B3LYP levels, respectively, and −0.16 ppm (HF) and −0.14 ppm (B3LYP) for the ^{1}H shielding constant. The quantum mechanically calculated correction is much larger, −12.04 ppm for ^{17}O, including −11.66 ppm zero-point vibrational and −0.38 ppm thermal contributions. For ^{1}H, the quantum mechanical correction is −0.549 ppm, consisting of −0.522 ppm zero-point vibration and −0.027 ppm thermal contributions.[20]

4.3. Average Shielding Tensors. Figures 5 and 6 present the full average nuclear magnetic shielding tensors of ^{17}O and ^{1}H in water in gaseous and liquid states, at the HF and B3LYP levels of theory, and at the temperature 300 K. It can be seen that, at both levels of theory, the average shielding tensors for oxygen in the gaseous state are diagonal, as appropriate for the C_{2v} site symmetry. The diagonal character is also visible in the liquid state, at least if doubled error limits are employed. It can be noticed that two of the diagonal components of $\boldsymbol{\sigma}^{^{17}\mathrm{O}}$, σ_{xx}, and σ_{zz} decrease a little when going from HF to B3LYP, but the component σ_{yy} along the molecular C_2 axis increases in the gas-state tensor. The net effect is a slight decrease in the shielding constant, when passing from HF to B3LYP. All the diagonal components of $\boldsymbol{\sigma}^{^{17}\mathrm{O}}$ decrease appreciably when passing from the gaseous state to the liquid state. At the B3LYP level, this decrease is more noticeable, as can also be seen in the gas-to-liquid shift which is larger for B3LYP.

The $\boldsymbol{\sigma}^{^{1}\mathrm{H}}$ tensors have two nonzero off-diagonal components, σ_{xy} and σ_{yx}, as the hydrogen site-symmetry is C_s. The other off-diagonal components are zero also in the liquid state, within doubled error limits. The diagonal components decrease when going from gas to liquid, but the off-diagonal components increase, the relative change being quite significant for the latter. The $\boldsymbol{\sigma}^{^{1}\mathrm{H}}$ tensor components behave almost identically at both HF and B3LYP levels, when passing from the gaseous state to liquid. This is also the reason the isotropic gas-to-liquid shifts are very close to each other at both computational levels.

4.4. ^{17}O Shielding Anisotropy and Asymmetry Parameter. Table 3 displays the ^{17}O nuclear shielding anisotropy and asymmetry parameter in water. We have two different results for these quantities due to different methods used in the averaging. Method 1 involves calculating the values of the parameters from the principal components of the diagonalized average shielding tensor (discussed above), while, in method 2, $\Delta\sigma$ and η are calculated from the principal components of the diagonalized tensors of each instantaneous cluster snapshot. In this case, the averaging is performed *after* the diagonalization

Table 3. ^{17}O Nuclear Shielding Anisotropy,[a] $\Delta\sigma$, and Asymmetry Parameter, η, in Water

method	$\Delta\sigma$(g)	$\Delta\sigma$(l)	$\Delta\sigma$(l) − $\Delta\sigma$(g)
HF[b]	50.6	34.4	−16.2
HF[c]	52.4 ± 0.2	38.3 ± 0.5	−14.1 ± 0.7
B3LYP[b]	48.0	33.3	−14.7
B3LYP[c]	50.1 ± 0.2	38.3 ± 0.6	−11.9 ± 0.7
HF[d]	52.1	33.1	−19.0
RASSCF[e]	46.94		
method	**η(g)**	**η(l)**	**η(l) − η(g)**
HF[f]	0.0124	0.0159	0.003
HF[g]	0.0287 ± 0.0008	0.0506 ± 0.0013	0.022 ± 0.003
B3LYP[f]	0.0366	0.029	−0.007
B3LYP[g]	0.0359 ± 0.0013	0.060 ± 0.002	0.024 ± 0.003
RASSCF[e]	0.0257		

[a] In ppm. [b] Present work. Method 1; the anisotropy is calculated from the diagonalized average shielding tensor as $\Delta\sigma = \sigma_{33} - {}^1/_2(\sigma_{22} + \sigma_{11})$, where the principal components are arranged as $\sigma_{33} > \sigma_{22} > \sigma_{11}$. The values for the anisotropy of an isolated molecule at the equilibrium geometry are 51.91 ppm (HF) and 49.53 ppm (B3LYP). [c] Present work. Method 2; the anisotropy is the average of individual anisotropies calculated from the principal components of the individual shielding tensors of the snapshot clusters. This method also yields the statistical error limit corresponding to the standard deviation of the mean value. [d] See footnote *f* in Table 1. [e] Reference 20. The equilibrium geometry values, for an isolated molecule, of the anisotropy and the asymmetry parameter are 49.33 ppm and 0.0323, respectively. Thus, the quantum mechanical rovibrational contributions to the anisotropy and asymmetry are −2.39 ppm and −0.0066, respectively. [f] Present work. Method 1; the asymmetry calculated using the same method as that described in footnote *b* for the anisotropy, using the formula $\eta = (\sigma_{22} - \sigma_{11})/\sigma_{33}$. The values of the asymmetry parameter at the equilibrium geometry are 0.0149 (HF) and 0.0383 (B3LYP), for an isolated molecule. [g] Present work. Method 2; the asymmetry calculated using the same method as that described in footnote *c* for the anisotropy.

step. Method 2 also yields statistical error limits for the parameters. While method 1 can be identified as corresponding to the determination of these parameters from static NMR experiments in an anisotropic medium, method 2 corresponds better to a relaxation experiment. Method 1 uses the Eckart coordinate system to average the individual shielding tensor components and, hence, yields the anisotropy and asymmetry parameter defined with respect to a static axis in this molecule-fixed frame. For ^{17}O, this direction is the *x* axis of the present choice of coordinate system, i.e., in the plane of the molecule and perpendicular to the C_2 axis. σ_{xx} is the largest principal component of the average oxygen shielding tensor, Figure 5. Method 2 produces the average of the individual parameters determined in the instantaneous principal axis systems of the shielding tensor, not coinciding with any fixed coordinate system attached to the molecule. Thus, the averaging in this method does not lead to parameters defined with respect to a particular axis. For the anisotropy, method 2 yields larger values in each case. For further discussions of the relation of the theoretically calculated and experimental (based on relaxation data) anisotropic NMR properties, we refer to refs 9 and 21.

The oxygen shielding anisotropy decreases when passing from the gaseous state to the liquid state, the difference being smaller in magnitude in method 2. The asymmetry parameter does not have a definite behavior, but the HF and B3LYP values are almost equal with method 2. No experimental results can be found in the literature. The single computational result for a static pentamer surrounded by a dielectric medium[53] is quite close to our results for the ^{17}O anisotropy in the two states.

We have at our disposal the equilibrium geometry values and the rovibrationally averaged values of the ^{17}O shielding anisotropy and the asymmetry parameter for a free (or gas-state) water molecule, calculated at three different levels: HF and B3LYP using classical rovibrational averaging, as well as RASSCF, where quantum mechanical rovibrational averaging was employed.[20] An estimate for the electron correlation effect at the equilibrium geometry (appropriate to the underlying BLYP/CPMD method of generating the trajectories) is obtained as the difference between the B3LYP and HF values and amounts to −2.38 ppm and 0.0234 for the anisotropy and the asymmetry parameter, respectively. From the results obtained by method 1, the corresponding correlation contributions in the rovibrationally averaged, gas-state values are very similar, −2.6 ppm and 0.0242. The difference between the classical and quantum mechanical rovibrational averaging can be estimated based on a comparison of the present B3LYP results with the RASSCF values of ref 20. While the classical averaging, used in connection with the current B3LYP calculations, results in the corrections of −1.5 ppm and −0.0017 for $\Delta\sigma$ and η, respectively, a quantum mechanical treatment of the nuclear dynamics gives the larger respective corrections of −2.4 ppm and −0.0066. By method 2, the rough correlation effects on $\Delta\sigma$ and η amount to −2.3 ppm and 0.0072, respectively. The results reported in ref 20 correspond to the present averaging method 1 (first averaging, followed by diagonalization); hence, comparison of the effects due to classical and quantum mechanical nuclear dynamics is meaningless for method 2. In conclusion, the correlated treatment tends to lower the anisotropy and increase the asymmetry parameter of ^{17}O shielding for gaseous water. Classical rovibrational averaging underestimates the magnitude of the rovibrational corrections.

For the ^{17}O anisotropy and asymmetry parameter in the liquid state, we can estimate the effect of electron correlation only, as the difference between the HF and B3LYP results. Correlation-induced changes amount, for the shielding anisotropy, to −1.1 ppm and 0.0 ppm with methods 1 and 2, respectively. The correlation effect on the asymmetry parameter is 0.0131 with method 1 and 0.0094 with method 2. Correlation slightly decreases the magnitude of the anisotropy and increases the asymmetry parameter with method 1. The effects of electron correlation in the gaseous and liquid states are not identical.

4.5. ^{1}H Shielding Anisotropy and Asymmetry Parameter. Table 4 displays the ^{1}H nuclear shielding anisotropy and asymmetry parameter in water. The estimated correlation effects on $\Delta\sigma$ and η at the equilibrium geometry are −1.33 ppm and 0.0042, respectively, as well as −1.34 ppm and 0.0044 in the rovibrationally averaged gas-phase state (method 1). Similar observations apply to method 2. Hence, correlation decreases the anisotropy of ^{1}H shielding in gaseous water. It also slightly increases the corresponding asymmetry parameter. The differences between the classical (B3LYP, −0.26 ppm and 0.0020 for $\Delta\sigma$ and η, respectively) and quantum mechanical (RASSCF, −1.079 ppm and 0.0068[20]) rovibrational averaging are again clear. Quantum dynamics leads to larger rovibrational contributions than the classical dynamics.

(50) Wasylishen, R. E.; Bryce, D. L. *J. Chem. Phys.* **2002**, *117*, 10061.
(51) Cazzoli, G.; Dore, L.; Puzzarini, C.; Beninati, S. *Phys. Chem. Chem. Phys.* **2002**, *4*, 3575.
(52) Sundholm, D.; Gauss, J.; Schäfer, A. *J. Chem. Phys.* **1996**, *105*, 11051.
(53) Mikkelsen, K. V.; Ruud, K.; Helgaker, T. *Chem. Phys. Lett.* **1996**, *253*, 443.

Table 4. ^{1}H Nuclear Shielding Anisotropy,[a] $\Delta\sigma$, and Asymmetry Parameter, η, in Water

method	$\Delta\sigma$(g)	$\Delta\sigma$(l)	$\Delta\sigma$(l) − $\Delta\sigma$(g)
HF[b]	17.42	27.3	9.9
HF[c]	17.46 ± 0.07	28.0 ± 0.2	10.6 ± 0.3
B3LYP[b]	16.08	25.7	9.7
B3LYP[c]	16.12 ± 0.08	26.5 ± 0.2	10.3 ± 0.3
expt[d]		27.4 ± 0.1	
expe[e,f] (ice)		34.0 ± 4.0	
expt[f,g] (ice)		34.2 ± 1.0	
expt[f,h] (ice)		28.7 ± 2.0	
expt[f,i] (ice)		28.5 ± 1.0	
HF[j]	20.29	31.73	11.44
HF[k]		34.83	
RASSCF[l]	19.08		

method	η(g)	η(l)	η(l) − η(g)
HF[m]	0.0450	0.0325	−0.013
HF[n]	0.0445 ± 0.0005	0.0545 ± 0.0012	0.010 ± 0.002
B3LYP[m]	0.0494	0.0346	−0.015
B3LYP[n]	0.0491 ± 0.0006	0.0566 ± 0.0013	0.008 ± 0.002
HF[k]		0.0047	
RASSCF[l]	0.04052		

[a] In ppm. [b] Present work. Method 1; see footnote *b* in Table 3. The principal axes of the average shielding tensor for the gaseous state at the B3LYP level are a_1 = (0.0000, 0.0000, 1.0000), a_2 = (−0.5057, 0.8626, 0.0000), and a_3 = (0.8626, 0.5057, 0.0000) expressed in the coordinate system specified in Figure 5. For the liquid state, the directions are a_1 = (−0.0129, 0.0226, 0.9996), a_2 = (−0.5530, 0.8327, −0.0260), and a_3 = (0.8330, 0.5531, −0.0017). The corresponding principal axes at the HF level do not deviate much from these. The values for the anisotropy at the equilibrium geometry are 17.67 ppm (HF) and 16.34 ppm (B3LYP). [c] Present work. Method 2; see footnote *c* in Table 3. [d] Reference 21 using relaxation data. [e] Reference 22. [f] The results for ice are from various temperatures. [g] Reference 23. [h] Reference 24. [i] Reference 25. [j] See footnote *f* in Table 1. [k] Reference 54. Using icelike water clusters containing 17 molecules at the temperature 0 K. [l] Reference 20. The equilibrium geometry values of the ^{1}H anisotropy and the ^{1}H asymmetry are 20.159 ppm and 0.3369, respectively. Thus the quantum mechanical rovibrational contributions to the anisotropy and asymmetry are −1.079 ppm and 0.0068. [m] Present work. Method 1; see footnote *f* in Table 3. The values for the asymmetry parameter at the equilibrium geometry are 0.0433 (HF) and 0.0474 (B3LYP). [n] Present work. Method 2; see footnote *g* in Table 3.

For the liquid-state water, the estimate for the effect of electron correlation on the ^{1}H shielding anisotropy is −1.6 ppm with method 1 and −1.5 ppm with method 2. The corresponding effect for the asymmetry parameter is 0.0021 with both averaging methods. In general, condensation from the gaseous to liquid state increases the anisotropy appreciably. The change is almost the same at both HF and B3LYP levels. Condensation decreases the asymmetry parameter when evaluated with method 1 but increases it with method 2.

We are only aware of one experimental result for ^{1}H nuclear magnetic shielding anisotropy in liquid water,[21] obtained from relaxation data. As indicated above, the anisotropy calculated using method 2 corresponds to the anisotropy contributing to the relaxation rate. The experimental anisotropy is between our calculated HF and B3LYP results. The experimental results for the ^{1}H anisotropy in ice are also shown for comparison in Table 4. The ^{1}H shielding anisotropy in water increases first upon condensation into liquid and further upon freezing. Static cluster model calculations[53] where the central molecule is explicitly solvated by four surrounding molecules and a dielectric continuum result in larger, more "icelike" anisotropy than the presently calculated, liquid-state values.

4.6. Quadrupole Coupling in Liquid and Gaseous State Water. Figures 7 and 8 contain the average ^{17}O and ^{2}H nuclear quadrupole coupling tensors in both gaseous and liquid states,

$$\chi^{\mathrm{HF}}_{^{17}\mathrm{O}}(e) = \begin{pmatrix} -9.64 & 0.00 & 0.00 \\ 0.00 & -1.71 & 0.00 \\ 0.00 & 0.00 & 11.35 \end{pmatrix}$$

$$\chi^{\mathrm{HF}}_{^{17}\mathrm{O}}(g) = \begin{pmatrix} -9.64 \pm 0.04 & 0.00 \pm 0.02 & 0.00 \pm 0.00 \\ 0.00 \pm 0.02 & -1.77 \pm 0.05 & 0.00 \pm 0.00 \\ 0.00 \pm 0.00 & 0.00 \pm 0.00 & 11.42 \pm 0.03 \end{pmatrix}$$

$$\chi^{\mathrm{HF}}_{^{17}\mathrm{O}}(l) = \begin{pmatrix} -7.74 \pm 0.05 & 0.07 \pm 0.05 & -0.03 \pm 0.02 \\ 0.07 \pm 0.05 & -0.83 \pm 0.05 & -0.01 \pm 0.03 \\ -0.03 \pm 0.02 & -0.01 \pm 0.03 & 8.56 \pm 0.05 \end{pmatrix}$$

$$\chi^{\mathrm{B3LYP}}_{^{17}\mathrm{O}}(e) = \begin{pmatrix} -8.88 & 0.00 & 0.00 \\ 0.00 & -1.81 & 0.00 \\ 0.00 & 0.00 & 10.69 \end{pmatrix}$$

$$\chi^{\mathrm{B3LYP}}_{^{17}\mathrm{O}}(g) = \begin{pmatrix} -8.88 \pm 0.04 & 0.00 \pm 0.02 & 0.00 \pm 0.00 \\ 0.00 \pm 0.02 & -1.87 \pm 0.05 & 0.00 \pm 0.00 \\ 0.00 \pm 0.00 & 0.00 \pm 0.00 & 10.75 \pm 0.03 \end{pmatrix}$$

$$\chi^{\mathrm{B3LYP}}_{^{17}\mathrm{O}}(l) = \begin{pmatrix} -6.94 \pm 0.05 & 0.08 \pm 0.05 & -0.02 \pm 0.02 \\ 0.08 \pm 0.05 & -0.83 \pm 0.05 & -0.01 \pm 0.03 \\ -0.02 \pm 0.02 & -0.01 \pm 0.03 & 7.77 \pm 0.05 \end{pmatrix}$$

Figure 7. Same conditions as those in Figure 5 but for ^{17}O nuclear quadrupole coupling tensor χ in MHz.

$$\chi^{\mathrm{HF}}_{^{2}\mathrm{H}}(e) = \begin{pmatrix} 122.6 & 173.3 & 0.0 \\ 173.3 & 23.2 & 0.0 \\ 0.0 & 0.0 & -145.8 \end{pmatrix}$$

$$\chi^{\mathrm{HF}}_{^{2}\mathrm{H}}(g) = \begin{pmatrix} 121.0 \pm 1.4 & 171 \pm 3 & 0.0 \pm 0.0 \\ 171 \pm 3 & 22.6 \pm 0.7 & 0.0 \pm 0.0 \\ 0.0 \pm 0.0 & 0.0 \pm 0.0 & -143.8 \pm 1.4 \end{pmatrix}$$

$$\chi^{\mathrm{HF}}_{^{2}\mathrm{H}}(l) = \begin{pmatrix} 92.2 \pm 1.0 & 127.0 \pm 1.4 & -0.3 \pm 0.3 \\ 127.0 \pm 1.4 & 14.1 \pm 0.5 & -0.07 \pm 0.14 \\ -0.3 \pm 0.3 & -0.07 \pm 0.14 & -106.3 \pm 1.0 \end{pmatrix}$$

$$\chi^{\mathrm{B3LYP}}_{^{2}\mathrm{H}}(e) = \begin{pmatrix} 120.7 & 168.6 & 0.0 \\ 168.6 & 21.0 & 0.0 \\ 0.0 & 0.0 & -141.7 \end{pmatrix}$$

$$\chi^{\mathrm{B3LYP}}_{^{2}\mathrm{H}}(g) = \begin{pmatrix} 119.6 \pm 1.4 & 166 \pm 3 & 0.0 \pm 0.0 \\ 166 \pm 3 & 20.4 \pm 0.7 & 0.0 \pm 0.0 \\ 0.0 \pm 0.0 & 0.0 \pm 0.0 & -139.8 \pm 1.4 \end{pmatrix}$$

$$\chi^{\mathrm{B3LYP}}_{^{2}\mathrm{H}}(l) = \begin{pmatrix} 91.8 \pm 1.0 & 125.7 \pm 1.4 & -0.3 \pm 0.3 \\ 125.7 \pm 1.4 & 12.6 \pm 0.5 & -0.07 \pm 0.14 \\ -0.3 \pm 0.3 & -0.07 \pm 0.14 & -104.4 \pm 0.9 \end{pmatrix}$$

Figure 8. Same conditions as those in Figure 7 but for ^{2}H nuclear quadrupole coupling tensor in kHz.

at the HF and B3LYP levels. While the underlying classical trajectories were obtained for the $^1H_2{}^{16}O$ isotopomer, the results are indicative of the medium effect, at least in the realm of classical mechanics, also for $^2H_2{}^{17}O$. The difference in the structures of water between path-integral CPMD simulations of $^1H_2{}^{16}O$ and $^2H_2{}^{16}O$ is smaller than that between either of these and a classical CPMD simulation.[55] The gaseous ^{17}O tensors are diagonal, similarly to the corresponding liquid-state tensors provided that doubled error limits are employed in the

Table 5. ^{17}O Nuclear Quadrupole Coupling Constant,[a] χ, and Asymmetry Parameter, η, in Water[b]

method	χ(g)	χ(l)	χ(l) − χ(g)
HF[c]	11.42	8.56	−2.85
HF[d]	11.42 ± 0.03	5.9 ± 0.4	−5.5 ± 0.4
B3LYP[c]	10.75	7.77	−2.98
B3LYP[d]	10.75 ± 0.03	5.55 ± 0.3	−5.2 ± 0.4
expt	10.2[e]	8.96[f], 8.0 ± 0.2[g]	
HF[h]		8.9 ± 0.3	

method	η(g)	η(l)	η(l) − η(g)
HF[i]	0.689	0.81	0.12
HF[j]	0.695 ± 0.007	0.51 ± 0.04	−0.18 ± 0.04
HF[k]	0.691	0.75	0.06
B3LYP[i]	0.652	0.79	0.13
B3LYP[j]	0.657 ± 0.007	0.51 ± 0.04	−0.15 ± 0.04
B3LYP[k]	0.653	0.73	0.08
expt[e]	0.75		
HF[g]		0.72	

[a] In MHz. [b] For references to more results from the literature, see ref 8. [c] Present work. Method 1; see footnote *b* in Table 3. The largest principal component of the diagonalized average tensor is quoted. The equilibrium geometry values for χ are 11.35 MHz (HF) and 10.69 MHz (B3LYP). [d] Present work. Method 2; see footnote *c* in Table 3. The average of the largest (in absolute value) principal components of the diagonalized EFG tensors of individual snapshot clusters is quoted. [e] Reference 56. The result obtained using beam-laser spectroscopy. [f] Reference 57. The result is determined from experimental chemical shift measurements and correlations between chemical shifts and quadrupole coupling constants. [g] Reference 58. [h] Reference 5. [i] Present work. Method 1; see footnote *b* in Table 3. The equilibrium geometry values for η are 0.698 (HF) and 0.661 (B3LYP). [j] Present work. Method 2; see footnote *c* in Table 3. [k] Present work. Method 3; the asymmetry calculated using the averages of the principal components of the individual EFG tensors.

latter. The average ^{2}H tensors have two equal nondiagonal components, since the site symmetry of hydrogen in the water molecule is C_s and $\boldsymbol{\chi}$ is a symmetric tensor by definition. The other off-diagonal components are zero. All the components decrease in magnitude upon condensation. The inclusion of correlation decreases the magnitude of each component.

Tables 5 and 6 display the ^{17}O and ^{2}H NQCCs and the associated asymmetry parameters of the nuclear quadrupole coupling tensor. As with the calculation of the anisotropy and asymmetry of the shielding tensors, different methods of averaging were used. Method 1 corresponds to first averaging the full $\boldsymbol{\chi}$ tensor, with the NQCC and the asymmetry parameter calculated from the subsequently obtained diagonal elements of the average tensor. Method 2 corresponds to averaging the NQCC (largest principal value of $\boldsymbol{\chi}$) and η obtained individually from each snapshot cluster calculation. For the asymmetry parameter, also a third method (method 3) was used, where η was calculated using the averaged principal components, obtained by averaging the principal components of the individual tensors appropriate to the snapshot clusters. Methods 2 and 3 automatically yield identical values for $\Delta\sigma$.

^{17}O NQCC at the HF level for a single molecule obtains similar values with both methods 1 and 2, and the same applies also for B3LYP. The effect of correlation approximated by the difference between the HF and B3LYP values is −0.67 MHz. In the liquid state, the two averaging methods yield very different results. The difference between the gaseous and liquid states is about 3 MHz (method 1) and above 5 MHz (method 2), at both HF and B3LYP levels. Eggenberger et al.[5] calculated the liquid-state value 8.9 ± 0.3 MHz, which is very close to the experimental value 8.96 MHz obtained by Ropp et al..[57] Our data are in much worse agreement with the experiment, mainly due to the fact that our basis sets are adapted for the less demanding task of calculating the nuclear shielding. In contrast, ref 5 employed basis sets specially designed for calculations of NQCC. In addition, an empirical scaling factor was used in ref 5, based on calibration calculations of ^{17}O NQCCs in the gas phase. Our present, completely nonempirical data should nevertheless provide a consistent gas-to-liquid *shift* of the NQCC and the full tensor. The ^{17}O asymmetry parameter for a single molecule obtains similar values with all three averaging methods, and both at HF and B3LYP levels. In the liquid state, methods 1 and 3 yield similar results, differing from the much lower value obtained with method 2. Furthermore, this makes the shift between the gaseous and liquid states have the opposite sign in method 2.

Table 6. ^{2}H Nuclear Quadrupole Coupling Constant,[a] χ, and Asymmetry Parameter, η, in Water

method	χ(g)	χ(l)	χ(l) − χ(g)
HF[b]	249	186	−64
HF[c]	250 ± 3	186 ± 2	−63 ± 4
B3LYP[b]	243	184	−59
B3LYP[c]	243 ± 3	184 ± 2	−59 ± 4
expt	308[d]	247[e]	
HF[f]	325.2 ± 0.3	267.3 ± 0.1	−57.9 ± 0.4
HF[g]		256 ± 5	

method	η(g)	η(l)	η(l) − η(g)
HF[h]	0.1526	0.1436	−0.009
HF[i]	0.1540 ± 0.0009	0.1463 ± 0.0015	−0.008 ± 0.003
HF[j]	0.1511	0.1441	−0.007
B3LYP[h]	0.1498	0.1353	−0.015
B3LYP[i]	0.1512 ± 0.0009	0.1376 ± 0.0014	−0.014 ± 0.003
B3LYP[j]	0.1483	0.1358	−0.012
expt[d]	0.14		
HF[g]		0.164 ± 0.003	

[a] In kHz. [b] Present work. Method 1; see footnote *c* in Table 5. The equilibrium geometry values for χ are 253 kHz (HF) and 247 kHz (B3LYP). [c] Present work. Method 2; see footnote *d* in Table 5. [d] See footnote *e* in Table 5. [e] Reference 57. See footnote *f* in Table 5. [f] Reference 9. Extensive classical simulation trajectory analyzed in terms of precalculated ab initio EFG data for ^2H_2O dimer, applied in the assumption of pairwise additivity. [g] Reference 4. Cluster calculations sampled from an MD simulation, including 82 pentamers. [h] Present work. Method 1; see footnote *b* in Table 3. The equilibrium geometry values for η are 0.152 (HF) and 0.149 (B3LYP). [i] Present work. Method 2; see footnote *j* in Table 5. [j] Present work. Method 3; see footnote *k* in Table 5.

For ^{2}H NQCC, the different averaging methods yield the same values in all cases, the correlation effect estimated at about −6 kHz and −2 kHz in the gaseous and liquid states, respectively. The computed shift between the states is very close to the difference between the experimental values for the gaseous and liquid states, −61 kHz. Hence, despite the fact that our calculation is not near the basis set limit for this property, changes in the chemical environment of the nucleus still remain well-reproduced. The environmental influence on the EFG at the nuclear site is not expected to be strongly dependent on the presence of very steep basis functions, and indeed our calculations reproduce the experimental gas-to-liquid shift of the ^{2}H

(54) Hinton, J. F.; Guthrie, P.; Pulay, P.; Wolinski, K. *J. Am. Chem. Soc.* **1992**, *114*, 1604.
(55) Chen, B.; Ivanov, I.; Klein, M. L.; Parrinello, M. *Phys. Rev. Lett.* **2003**, *91*, 215503.
(56) Verhoeven, J.; Dymanus, A.; Bluyssen, H. *J. Chem. Phys.* **1969**, *50*, 3330.
(57) Ropp, J.; Lawrence, C.; Farrar, T. C.; Skinner, J. L. *J. Am. Chem. Soc.* **2001**, *123*, 8047.
(58) van der Maarel, J. R. C.; Lankhorst, D.; de Bleijser, J.; Leyte, J. C. *Chem. Phys. Lett.* **1985**, *122*, 541.

NQCC equally well as the recent study,[9] where such functions were used. The analysis of ref 9 reveals that roughly one-half of the solvation effect on this property is due to direct environmental effects, i.e., intermolecular contributions to the EFG. The other half has its origin then in the indirect effect via solvation-induced modification of the average structure of the monomer.

In ref 9, it was further suggested that, due to the assumptions made in the analysis of experimental NMR relaxation data, the χ(l) value may be too small by 15 kHz. This would render the experimental χ(l) − χ(g) to equal ca. −46 kHz, with error limits of about ±10 kHz. The results of the present paper as well as those of ref 9 almost fall within the error limits also after the suggested revision of the experimental data. We conclude that the experimental situation concerning χ(l) remains unclear, but our calculations are at least qualitatively correct for the gas-to-liquid shift of ^{2}H NQCC.

The ^{2}H asymmetry parameter is calculated to be about 0.15 in the gaseous state, the experimental value being 0.14. The correlation effect in the gaseous and liquid states is about −0.003 and −0.008, respectively. The gas-to-liquid shift becomes larger at the B3LYP level than with HF, due to the unequal effect of correlation in the gaseous and liquid states.

5. Conclusions

We have presented completely nonempirical calculations of the ^{17}O and ^{1}H nuclear magnetic shielding tensors as well as ^{17}O and ^{2}H nuclear quadrupole coupling tensors of water in the liquid and gaseous states, at 300 K. The calculations employed the Hartree−Fock (HF) and density functional theory (DFT) levels, the latter using the hybrid B3LYP functional. First principles molecular dynamics (MD) simulation by the Car−Parrinello method was used to produce instantaneous configurations of water molecules. Clusters including different numbers of molecules were cut out of the simulation snapshots. Subsequently, quantum chemical calculations were performed to obtain the property tensors for the central molecule of each cluster. Gaseous state water was represented by the snapshots from a MD simulation for a single molecule.

At the B3LYP level, ^{17}O nuclear magnetic shielding constants for the gaseous and liquid states are found to be 309.7 ± 0.9 ppm and 268.5 ± 0.6 ppm, respectively, leading to the gas-to-liquid shift of −41.2 ± 1.4 ppm. For ^{1}H, the corresponding results are 30.07 ± 0.05 ppm and 24.80 ± 0.08 ppm, leading to the shift of −5.27 ± 0.13 ppm. These shifts exceed the magnitude of the experimental values by about 5 ppm for ^{17}O and 1 ppm for ^{1}H. The electron correlation effect, estimated by the difference between B3LYP and HF results, is large for ^{17}O, as a much smaller gas-to-liquid shift is obtained at the uncorrelated HF level for this nucleus. As particular care has been taken of the statistical sampling and the balance of the different error sources, these gas-to-liquid shift values should be representative of the performance of the HF and B3LYP levels of theory.

Nuclear quadrupole coupling constants for ^{17}O for the gaseous and liquid states, at the B3LYP level, are 10.75 MHz and 7.77 MHz, respectively, the change between the states being −2.98 MHz. The corresponding ^{2}H results are 243 kHz and 184 kHz, and the shift is −59 kHz. The deuterium values are relatively close to the experimental results, but the oxygen values differ appreciably, due to the basis sets used.

For the first time, full thermally averaged nuclear shielding and quadrupole coupling tensors are reported for both nuclei in both gaseous and liquid states, enabling shifts in the individual tensor components to be observed upon the phase transition. Different methods were employed to obtain the anisotropic spectral parameters from the tensors. The parameters obtained using the *average tensors*, expressed in the Eckart frame common to all instantaneous configurations of the solvated molecule, are recognized to correspond to static NMR experiments. The parameters relevant to relaxation experiments are obtained using direct averaging of shielding anisotropies and quadrupole coupling constants, as well as the corresponding asymmetry parameters, regardless of a common reference frame. The results are in good agreement with the existing experimental data.

Further analysis of the gas-to-liquid shifts of the nuclear shielding and quadrupole coupling tensors in water, in terms of the local hydrogen bonding geometries and populations, is to be discussed elsewhere.

Acknowledgment. The authors are grateful to Prof. Kenneth Ruud (Tromsø) and Dr. Robert Berger (Berlin) for help with the DALTON software, Prof. Trygve Helgaker (Oslo) and Dr. Pawel Sałek (Stockholm) for access to a prerelease DFT version, and Dr. Juhani Lounila (Oulu) for useful discussions. We acknowledge financial support from the Ella och Georg Ehrnrooths Stiftelse (T.P. and J.V.), Magnus Ehrnrooth Foundation (T.P., A.S., and J.V.), Emil Aaltonen Foundation (J.V.), and The Academy of Finland (J.V., K.L., A.S., and J.J.). J.V. is Academy Fellow of The Academy of Finland. Computational resources were partially provided by the Center for Scientific Computing Ltd, Espoo, Finland.

JA048049I